university of groningen / faculty of science and engineering

Investigation of the capabilities and limitations of the Open Catalyst pre-trained machine learning models

Author:
Goos MULDER
(s4545257)

Supervisor:
dr. Andrea GIUNTOLI
Second examiner :
dr. Francesco MARESCA
Daily supervisor SKF:
dr. SEBASTIÁN ECHEVERRI RESTREPO

Bachelor's Thesis
To fulfill the requirements for the degree of
Bachelor of Science in Physics
at the University of Groningen

July 3, 2024

Contents

Page

Abstract **4**

Acknowledgements **5**

1 Introduction **6**

2 Background Literature **7**
2.1 Adsorption energy . . . 7
2.2 Density Functional Theory . . . 7
2.3 Machine learning in molecular dynamics . . . 9
2.3.1 Invariant Geometric GNNs . . . 10
2.3.2 Equivariant Geometric GNNs . . . 10
2.4 The Open Catalyst Project . . . 10
2.4.1 The OC20 Dataset . . . 11
2.5 Baseline GNN models . . . 12
2.5.1 Evaluation metrics . . . 12
2.5.2 EquiformerV2 . . . 13
2.5.3 Gemnet-OC . . . 13

3 Baseline papers **14**
3.1 Paper 1 . . . 14
3.1.1 DFT settings . . . 14
3.1.2 Structure definition . . . 14
3.2 Paper 2 . . . 15
3.2.1 DFT settings . . . 15
3.2.2 Structure definition . . . 15

4 Methodology **17**
4.1 Computational specifications . . . 17
4.2 Structure relaxations . . . 17
4.3 OCPCalculator . . . 17
4.4 Ammonia Nitrogen Reduction Reactions . . . 17
4.5 Fe(110) ZDDP . . . 18

5 Results and Discussion **19**
5.1 Nitrogen reduction reaction . . . 19
5.1.1 EquiformerV2 . . . 19
5.1.2 GemNet-OC-Large . . . 21
5.1.3 Nitrogen Reduction Reaction Discussion . . . 21
5.2 ZDDP adsorption on Iron (110) surface . . . 23
5.2.1 EquiformerV2 . . . 23
5.2.2 GemNet-OC-Large . . . 23
5.2.3 ZDDP adsorption on Iron (110) surface discussion . . . 25

6 Conclusion **26**

Bibliography **27**

A MACE calculations **32**

B Literature values **34**

Appendices **34**

Abstract

Adsorption energy is of great importance in material science. It refers to the energy released when a molecule adheres to a surface. Obtaining a system's adsorption energy can help understand the underlying mechanism of the system's macroscopic behaviour. Density Functional Theory is a widely used computational method for atomic and molecular simulations, including finding adsorption energies. DFT is an extremely computationally heavy iterative quantum mechanical simulation method. New approaches are being researched to avoid this computationally heavy method, including creating atomic force fields based on graph neural networks. The Open Catalyst Project is a collaborative project that aims to accelerates research into machine learning-based molecular dynamics models to assist or replace DFT. The project provides large datasets with over 1.2 million DFT relaxations and various pre-trained graph neural networks for the community to improve. This report contains an analysis of an invariant and equivariant model. Both models perform a set of relaxations on 19 bimetallic compounds with ammonia-base adsorbates. The mean absolute errors on these configurations for both models are found to be 1.0669 eV and 1.1066 eV for EquiformerV2 and GemNet-OC-Large, respectively. Additionally, relaxations of the more complex molecule, zinc dialkyl dithiophosphate (ZDDP), on an iron surface are performed, leading to incorrect outcomes. The models are found to be much faster when compared to DFT. However, much research is needed to obtain the desired accuracy.

Acknowledgments

First, I would like to thank SKF for allowing me to complete my bachelor's thesis with them. From SKF, I would specifically like to thank Dr. Sebastián Echeverri Restrepo for his positive attitude and fast communication and for familiarising me with the wonderful world of molecular and atomic simulations. Finally, I would like to thank the micromechanics research group, particularly my primary supervisor, Dr. Andrea Giuntoli, for his immense positive guidance and for opening my eyes to the joy of academic research.

1 Introduction

The concept of adsorption energy is of great importance in material science. It refers to the amount of energy released when a molecule adheres to a surface [1], where a negative adsorption energy indicates an energetically favourable reaction. This concept is crucial because a molecular interaction as such can significantly influence the system's macroscopic behaviour. For instance, the reaction rate of a catalyst is strongly influenced by the corresponding adsorption energy [2, 3]. Additionally, understanding adsorption energy can provide a deeper insight into complex interactions, such as the study of the most used anti-wear additive in the automotive industry [4], zinc dialkyl dithiophosphate (ZDDPs).

There are various methods of obtaining adsorption energies. They can be obtained through experiments and computational simulations. These simulations are often performed with Density Function Theory (DFT) [5], a quantum mechanical computation method that, using various approximations, estimates the total energy of the system and the forces on each atom for every iteration until an energy minimum is found [6]. A problem, however, with DFT is that the estimation of energies and forces is extremely computationally heavy, resulting in computations ranging from hours to days per relaxation on O(10–100) core CPUs [6]. A more computational-friendly approach could be using an atomic force field, a set of parameters and equations to describe the potential energy and forces between atoms based on their positions and chemical environments [7]. Unfortunately, these force fields lack the desired accuracy [8, 9].

Another promising method is machine learning, by creating a force field based on a graph neural network where the nodes represent the atoms and the edges between the notes embed the information of the bonds [10]. These machine learning-based molecular dynamics models, however, require an existential amount of DFT data for the models to be trained to reach the desired accuracy [11]. Fundamental AI Research (FAIR) at Meta AI and Carnegie Mellon University's (CMU) Department of Chemical Engineering have started a collaborative research project to accelerate the research in these models. They attempt to speed up the research by releasing an open software repository [1] containing the largest available dataset, including 1,281,040 DFT relaxations [11] and multiple pre-trained models for the community to continue building on.

This report investigates the capabilities and limitations of two of these readily available models. The models in question are an equivariant model, EquiformerV2 [12], and an invariant model, GemNet-OC-Large [13]. The first approach to show the capabilities of the models consists of performing a set of relaxations on configurations of bimetallic compounds with ammonia base adsorbates. The mean absolute errors on these configurations for both models are found to be 1.0669 eV and 1.1066 eV for EquiformerV2 and GemNet-OC-Large, respectively. Additionally, relaxations of ZDDP on an iron surface are performed to investigate the capability of the pre-trained models to extrapolate to systems not considered during training. However, all attempts to relax the ZDDP iron configuration led to incorrect outcomes. Interestingly to note are the computational efforts, as all relaxations performed were multiple orders of magnitude faster than the estimated DFT simulation times. The main objective of this report is to show the potential of these machine learning-based molecular dynamics models, particularly in terms of time efficiency, while stressing the need for ongoing research to improve their accuracy.

[1] https://github.com/FAIR-Chem/fairchem

2 Background Literature

2.1 Adsorption energy

Adsorption is the process of a particle or molecule attaching to a solid surface, where the adsorbate is the particle or molecule and the adsorbent is the solid [1]. An adsorption process can be either endothermic or exothermic. A measure of the strength of this process is referred to as the adsorption energy. Adsorption energy is the difference between the energy of a surface with an adsorbate and that of a separate surface and adsorbate. This generally is derived according to:

$$E_{\text{ads}} = E_{\text{surface+adsorbate}} - E_{\text{surface}} - E_{\text{adsorbate}}. \tag{1}$$

A negative adsorption energy indicates an energetically favourable adsorption process. This insight is crucial in understanding the behaviour of surface interactions.

2.2 Density Functional Theory

A widely used computational method for calculating adsorption energy is Density Functional Theory (DFT). This computational method is based on the fundamental laws of quantum mechanics [14]. Finding a solution to the time-independent, non-relativistic Schrödinger equation to be more exact:

$$H\psi = E\psi \tag{2}$$

Where H is the Hamiltonian, and ψ is a set of eigenstates or solutions of the Hamiltonian. The details of the Hamiltonian depend on the system in discussion. For some well-known examples, the Hamiltonian is simple, and the Shrödinger equation can be solved exactly. Considering a multi-body system with multiple electrons and nuclei interacting with each other results in a much more complicated Schrödinger equation, which can only be solved through numerous approximations. The first one is the Born-Oppenheimer approximation, which simplifies the Hamiltonian by stating that the nucleus is fixed with respect to the electron. This stems from the fact that the nucleus has more than 1800 times the mass of an electron [5]. Reducing the Hamiltonian to the electric Hamiltonian, which is a function of the spatial coordinates of each of the N electrons.

Finding the lowest ψ corresponding to the ground state is a non-trivial problem due to the term of electrostatic repulsion between each individual electron term, which is included in the electric Hamiltonian. ψ, however, can be approximated as a product of the individual wave functions,

$$\psi = \psi(r_1, \ldots, r_N) \approx \psi_1(r)\psi_2(r)\ldots\psi_N(r). \tag{3}$$

This is known as the Hartree product [5]. A closely related quantity is the electron density at a particular position $n(\mathbf{r})$. Which can be written as:

$$n(\mathbf{r}) = 2\sum_i \psi_i^*(r)\psi_i(r) \tag{4}$$

describing how many electrons, on average, will be found in this position, where the factor of 2 is a result of the Pauli exclusion principle. Now $n(\mathbf{r})$ is a function of only 3 coordinates whilst maintaining a lot of information from the full wave function, which is a function of 3N coordinates.

DFT theory rests on two fundamental theorems, both of which are derived and proven by Kohn and Hohenberg and derived by Kohn and Sham [5].

1. The ground-state energy E from Schrödinger's equation is a unique functional [2] of the electron density $n(\mathbf{r})$. that can be written as

$$E[\{\psi_i\}] = E_{\text{known}}[\{\psi_i\}] + E_{\text{XC}}[\{\psi_i\}]. \tag{5}$$

2. The electron density that minimizes the energy of the overall functional is the true electron density corresponding to the complete solution of the Schrödinger equation.

The functional shown in Equation 5 is split into two parts. Where the functional E_{known} contains all known terms, and E_{XC} is the eXchange-Correlation functional defined to include all the quantum mechanical effects that are not included in the known terms. Kohn and Sham showed that finding the right electron density can be expressed as solving a set of equations in which each equation involves only a single electron. This results in the Kohn-Sham equations,

$$\left[\frac{\hbar^2}{2m}\nabla^2 + V(\mathbf{r}) + V_H(\mathbf{r}) + V_{XC}(v)\right]\psi_i(\mathbf{r}) = \varepsilon_i\psi_i(\mathbf{r}). \tag{6}$$

Where $V(\mathbf{r})$ corresponds to the potential of the interaction between an electron and a collection of atomic nuclei, $V_H(\mathbf{r})$ is the Hartree potential, and $V_XC(\mathbf{r})$ is the potential that defines the exchange and correlations contributions to the single electron equations.

The following iterative process is used to find a solution to the Kohn-Sham equations [5]:

1. Define an initial trial electron density, $n(\mathbf{r})$.

2. Solve the Kohn–Sham equations defined using the trial electron density to find the single-particle wave functions, $\psi_i(\mathbf{r})$.

3. Calculate the electron density defined by the Kohn–Sham single-particle wave functions from step 2, $n_{\text{KS}}(\mathbf{r}) = 2\sum_i \psi_i^*(\mathbf{r})\psi_i(\mathbf{r})$.

4. Compare the calculated electron density, $n_{\text{KS}}(\mathbf{r})$, with the trial electron density used in solving the Kohn–Sham equations, $n(\mathbf{r})$. If the two densities are the same, then this is the ground-state electron density, and it can be used to compute the total energy. If the two densities are different, then the trial electron density must be updated in some way. Once this is done, the process begins again from step 2.

This iterative process is computationally heavy, especially because of the number of computations needed scale $O(n^3)$ with respect to the number of atoms in the structure [5]. The computational time of a single adsorbate-surface DFT relaxation considered in this report is approximately 24 hours, as mentioned in Lan et al. [15]. Given that multiple configurations are generally explored to determine the adsorption energy, the entire set of DFT calculations can span several days to weeks.

The exchange-correlation functional in the Kohn-Sham equation can only be derived exactly in one case [5]. This is in uniform electron gas, where the electron density is constant everywhere in space. This results in the most common approximation of the XC functional, the local density approximation (LDA). Another well-known functional is the generalized gradient approximation (GGA), which

[2] A functional takes a function as an input and outputs a single number.

utilises information about the local electron density and the local gradient in the electron density.

The two most widely used functionals in calculations involving solids are the Perdew–Wang [16] functional (PW91) and the Perdew–Burke–Ernzerhof [17] functional (PBE), both of which are GGA functionals. Various other GGA functionals have been developed and used, particularly for calculations with isolated molecules [5]. Different functionals will give moderately different results for any particular configuration of atoms. Another functional is the Revised Perdew–Burke–Ernzerhof [18] (RPBE), which is similar to the PBE but with a slight variation in parameter settings. The difference between PBE and RPBE is well studied [19, 18]; RPBE generally underestimates cohesive energies, resulting in an overestimation in surface stability, which corresponds to generally higher adsorption energy. Examining studies [20, 21, 22, 23] that report the adsorption energies using PBE and RPBE functionals reveals a discrepancy of approximately 0.30 to 0.60 eV in the calculated adsorption energies. These studies typically indicate the values for different functionals in their results.

2.3 Machine learning in molecular dynamics

In Molecular Dynamics (MD) simulations, force fields are essential for predicting the properties and functions of molecular systems [24]. These force fields describe the global potential energy surface (PES) within the Born-Oppenheimer (BO) approximation. Traditionally, the parameters for these force fields are derived from a set of DFT calculations or experimental data. However, these classical force fields often struggle with accuracy and reliability outside the conditions they were initially fitted for; this is a significant implication when researching new materials for their properties.

Machine learning (ML) techniques have been introduced to overcome these limitations [12, 13]. These ML approaches aim to model the global PES with higher accuracy across various materials and molecular sizes. ML models can learn detailed representations of potential energy surfaces using large datasets comprising numerous atomic configurations. However, these models require extensive data and are complex, making them less transparent and challenging to analyse. Conserving energy total energy can also be a problem for these models [25].

Machine learning algorithms are broadly classified into two categories: supervised and unsupervised models. Supervised models work with labelled data, where each input data point is associated with an output data point. On the other hand, unsupervised models operate on unlabelled data, where the input data does not correspond to the output [26]. This report will focus on supervised neural networks (NNs) and graph neural networks (GNNs).

Graphical Neural Networks (GNNs) are specifically designed to operate on graph-structured data, which consists of nodes (vertices) and edges (links) describing the relationship between entities, as shown in Figure 1. GNNs generally perform well for tasks where the data naturally forms a graph; atomic and molecular structures are a perfect example, where the nodes stand for atoms (or a set of atoms), and the edges represent chemical bonds [10]. These GNNs are becoming more widely studied in material science because they can accelerate the research of predicting material properties like DFT but with orders of magnitude larger computational speeds [27].

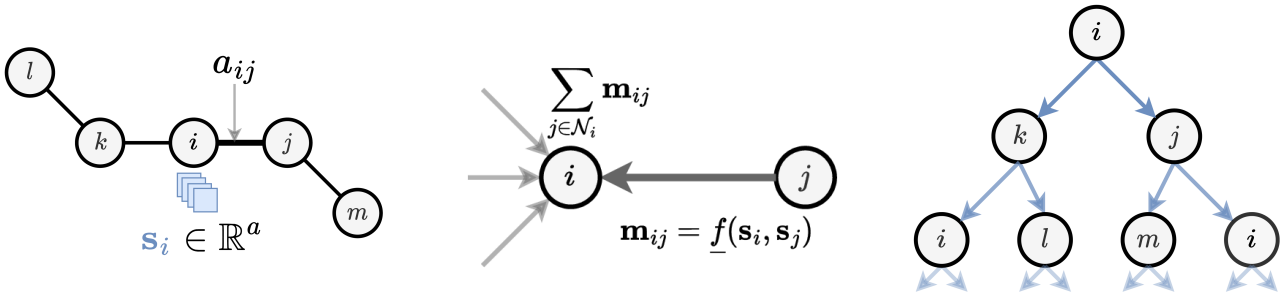

(a) An attributed graph (b) Message passing (c) GNN computation tree

Figure 1: Graphs and Graph Neural Networks. (a) Graphs model a set of entities as nodes, with edges denoting relationships and structure among them. (b) GNNs build latent representations of graph data through message passing operations, where each node performs learnable feature aggregation from its local neighbourhood. (c) Stacking L message passing layers enables GNNs to send and aggregate information from L-hop subgraphs around each node. Figure and caption taken from Duval et al. [25]

2.3.1 Invariant Geometric GNNs

Invariance describes the property of remaining unchanged under certain transformations or conditions. GNNs apply this when considering scalar quantities between atoms, such as pairwise distances, triplet-wise angles, and quadruplet-wise torsion angles [25]. These quantities are all invariant to Euclidean transformations, resulting in guaranteed invariant intermediate representations and predictions. In general, invariant GNNs rely heavily on precomputed procedures to scale geometric information. However, this introduces the problem of increasing the complexity of architectures when considering higher body order invariants.

2.3.2 Equivariant Geometric GNNs

Equivariant GNNs are designed to ensure that transformations applied to the input graph result in predictable, corresponding transformations of the features in the hidden layers [25]. Specifically, if the input graph is rotated, the features in the hidden layers will also rotate consistently. This property, known as equivariance, ensures that the model respects the symmetries of the input data. Unlike invariant models that pre-calculate local invariants, equivariant GNNs dynamically transform features during message passing, maintaining symmetry throughout the network.

2.4 The Open Catalyst Project

The Open Catalyst Project is an initiative to accelerate the research of new catalysts for renewable energy storage. It is a collaboration between Fundamental Research (FAIR) at META and Carnegie Mellon University (CMU). The project aims to grant the catalysis community access to a large and diverse dataset to train ML models [6].

The project's biggest goal is to offer a scalable, cost-effective solution to predicting the properties of catalysts by providing an open-source dataset containing over 1.3 million molecular relaxations resulting from over 260 million DFT calculations. Baseline GNN models are offered for the community to expand and improve. The calculations in the dataset are performed using Vienna Ab initio Simulation Package VASP [28].

The project is focused on catalysts because of their crucial role in the energy transition, especially for alternative energy storage solutions [30, 31]. Adsorption energy significantly impacts catalyst performance; too strong or weak adsorption can hinder efficiency [2, 3]. Hydrogen energy storage benefits greatly from catalysts, enhancing overall effectiveness [32]. Researchers use simulations, primarily DFT, to explore new catalytic materials [33]. However, DFT's high computational demands pose challenges, particularly for large-scale material screening [6]. Rapid advancements in renewable energy processes, such as fuel cells and ammonia production, rely on improved catalysis to meet urgent climate and energy needs [34], though catalyst discovery remains time-intensive. It is important to note that the name of their Python package was changed from Open Catalyst to Fairchem.

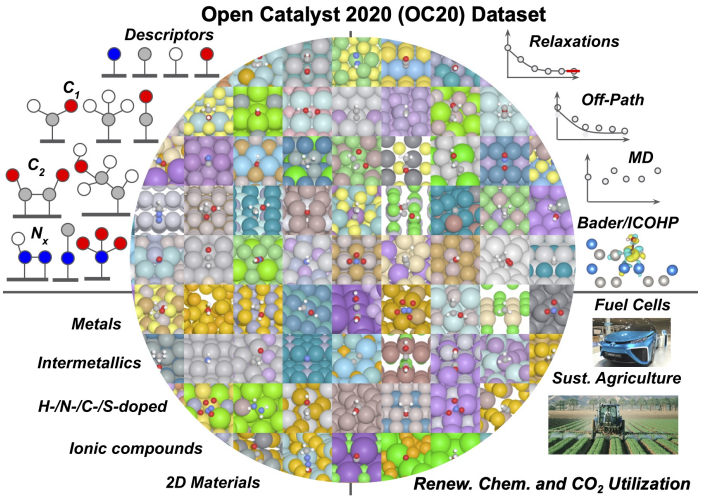

Figure 2: Adsorbates, materials, calculations, and impact areas of the OC20 dataset. Images are a random sample of the dataset. Figure and caption taken from Chanussot et al. [29]

2.4.1 The OC20 Dataset

The first data set of open catalysts consists of 640,081 relaxations with over 133 million intermediate training structures [29]. The dataset is built up in four stages:

1. Adsorbate selection
   A selection of 82 adsorbates is made based on their importance in energy applications. All 82 adsorbates are a combination of Oxygen, Hydrogen, Carbon, and Nitrogen. Oxygen and Hydrogen are important because of their presence in water-solvated electrochemical reactions; carbon is relevant because of solar fuel synthesis; and nitrogen is relevant because of solar fuel and solar-chemical synthesis.

2. Surface selection
   The surface structure is sampled randomly from the 11,451 materials in the Materials Project [35]. The unary, binary, and ternary percentages are 5%, 65%, and 30%, respectively. The symmetrically equal surfaces with miller indices less or equal to 2 are selected. In total, 55 elements were chosen: reactive nonmetals, alkali metals, alkaline earth metals, metalloids, transition metals, and post-transition metals. These bulk structures are all reoptimised with DFT to avoid differences in DFT settings from the Materials Project.

3. Initial structure generation
   Creating the initial structures and placing the adsorbates are all performed by ASE [28]. CatKit [36] locates the symmetrically distinct adsorption sites. From all configurations mentioned earlier, one is selected and used to create two inputs for the DFT calculations: One setup with the bulk and the adsorbate and one just with the catalyst bulk structure. This, in total, resulted

in 1,919,165 and 616,124 unique inputs. These were split up into train, validation and test validation split sets.

4. Structure relaxation
   The structure relaxations are all performed with the Vienna Ab Initio simulation pack (VASP) [28]. The structures are relaxed until all the forces on the atoms are below $0.03\,\mathrm{eV\,\AA^{-1}}$. Every relaxation was allowed up to 144 hours (12 cores) per calculation. Every intermediate structure, energy and force are saved for training and evaluation. Only the adsorbate and the surface atoms are free to move; the rest of the bulk atoms are constrained to their location; this is done to avoid unrealistic structure deformations. Selecting the correct DFT setting was complex and required careful consideration. The RPBE [17] level theory was chosen with no spin-polaristion considering the trade-off between accuracy and computational efficiency. The additional settings were chosen after thoroughly considering inconsistent cutoffs/settings and the representatives of typical numerical/convergence issues.

The adsorption energies are calculated according to:

$$E_{\mathrm{ad}} = E_{\mathrm{sys}} - E_{\mathrm{slab}} - E_{\mathrm{gas}} \tag{7}$$

Where E_{sys} is the DFT energy of the catalyst with the adsorbate, E_{slab} is the DFT energy of the surface, and E_{gas} is the gas-state energies of the adsorbate. The gas-state adsorbates are computed from a linear combination of N_2, H_2O, CO, and H_2. The linear combination O2 is purposely avoided because of the overrepresentation of the O-O bonds in GGA.

Roughly 872,00 adsorption energies were calculated, of which 3.7% are unary, 61.4% are binary, and 34.9% are on ternary catalysts. Of these catalysts, 28,9% contained reactive nonmetal elements, 8.1% alkali metals, 10.2% alkaline earth metals, 26.4% metalloids, 81.3% transition metals, and 37.2% post-transition metals. For the adsorbates, 6.6% had only oxygen or hydrogen; 25.2% had C1 adsorbates, 44.4% had C2 adsorbates, and 29.0% had nitrogen. Even though it is an extensive data set relative to other data sets, this data set only contains 18.9% of the total 27,775 possible compositions. For every composition, an average of 249 adsorption calculations were performed successfully. The open catalyst project has set a benchmark, requiring the energy and force estimates to be computed in approximately 10 ms. This represents a considerable leap forward from DFT's capabilities.

2.5 Baseline GNN models

The Open Catalyst project is not only involved in supplying the data set but also provides pre-trained models built on current state-of-the-art GNNs. All baseline ML approaches are built with Pytroch Geometric [37, 38], a library designed specifically for deep learning on graph-structured data. As previously mentioned, the nodes represent atoms, and the edges represent neighbouring atoms' relationships. For every node, the atom embedding is iteratively updated based on the message passed along the edges. The GNN models can be segmented into two groups: Invariant and equivariant.

2.5.1 Evaluation metrics

The Open Catalyst Project's website [3] has a public leaderboard encouraging model improvement. Specific test sets are used to obtain the evaluation metrics for the leaderboard, and the ground truth

[3] https://opencatalystproject.org/leaderboard.html

values are computed with DFT. The leaderboard has multiple evaluation metrics, the most important of which are EWT% and the Energy MAE (eV). The EWT% represents the energy within a threshold of the ground truth. The energy MAE is the Mean Absolute Error between the computed relaxed energy and the ground truth. The current statistics for the mentioned models are taken from their public leaderboard and presented in Table 1. The leaderboard is publicly available to encourage the community to improve these models further.

Model	**EWT (%)**	**ENERGY MAE (EV)**	**Date**
EquiformerV2 - 31M - LBFGS Fix	16.8	0.3009	2024/05/05
GemNet-OC-Large	14.97	0.3477	2022/07/14

Table 1: Leaderboard for Open Catalyst pre-trained models, last updated on 19-06-2024 from [39].

2.5.2 EquiformerV2

EquiformerV2 [12] is an equivariant model that currently outperforms previous state-of-the-art models. Additionally, the model offers a better speed-accuracy trade-off and reduces the number of DFT calculations needed to calculate adsorption energies by half [15]. One challenge in equivariant GNNs is the complexity of tensor products, which increases significantly as the model scales. EquiformerV2 uses eSCN convolution to simplify these tensor products with linear operations to address this [40]. This method aligns the input molecule along one axis, reducing the degrees of freedom to rotations around that axis, thus lowering computational costs.

2.5.3 Gemnet-OC

Gemnet-OC [13] is an invariant model designed to handle large systems by efficiently calculating quadruplet interactions and dihedral angles. It also considers the importance of long-range interactions. Based on the geometric message-passing neural network (GemNet) [41], Gemnet-OC improves upon regular message-passing neural networks by embedding direct edges between atoms. The model captures complete geometric information by updating atom and edge embeddings through multiple layers using neighbouring atom edge embeddings, including distances between atoms, angles between neighbouring edges, and dihedral angles defined by triplets of edges. This leads to a more accurate model with reduced training times compared to its predecessors.

3 Baseline papers

3.1 Paper 1

"Enhanced Catalytic Activity of Bimetallic Ordered Catalysts for Nitrogen Reduction Reaction by Perturbation of Scaling Relations"

This paper [42] investigates the catalytic activity of bimetallic catalysts in Nitrogen reduction reactions. This is done for a wide variety of bimetallic compounds. Research into ammonia is essential due to its great applicability in fertiliser and energy storage materials. The paper calculates various values for 29 A_3B alloys and 11 adsorbates. For this research, only the δE values are relevant. This paper was chosen because of the large amount of adsorption energies for bimetallic configurations, and the goals is to compare these values to those calculated by the ml-models. The models are expected to perform well on these configurations because the dataset on which the models are trained consists of 61.4% binary metals.

3.1.1 DFT settings

The DFT calculations were performed with VASP [43] and the PBE GGA [17] exchange-correlation functional. The long-range van der Waals (vdW) interaction was considered through the DFT-D3 [44] method, with an atomic-pairwise correction term added.

3.1.2 Structure definition

For the (111) surface, a (2x2) hexagonal in-plane lattice with four layers was defined. The two bottom atomic layers were constrained to their location, and a 15 Å vacuum layer was added in both vertical directions. A schematic is shown in Figure 4. The kinetic cutoff energy for the plane-wave basis was set to 400 eV, and the (3x3x1) Monkhorst-Pack [45] grid with the Γ-centered k-point sampling in the Brillouin zone was employed. The threshold criteria for energy was set to 1×10^{-5} eV and the force to 0.05 eV Å^{-1}.

The adsorption energy was calculated according to the following:

$$\begin{aligned}\Delta E(\mathrm{N}_x\mathrm{H}_y) = &\left(E(*\mathrm{N}_x\mathrm{H}_y) + (2-x)E(\mathrm{NH}_3(g)) + \frac{(3x-y)}{2}E(\mathrm{H}_2(g))\right) \\ &- \left(E(\mathrm{slab}) + E(\mathrm{N}_2(g)) + 3E(\mathrm{H}_2(g))\right),\end{aligned} \tag{8}$$

where $E(*N_xH_y)$, $E(\mathrm{slab})$, $E(\mathrm{N}_2(g))$, $E(\mathrm{H}_2(g))$, and $E(\mathrm{NH}_3(g))$ represent the total energies of the substrate with the adsorbed intermediate, the clean substrate, gas-phase N_2, gas-phase H_2, and gas-phase NH_3, respectively.

The selected 19 compounds and 9 adsorbates are shown in Table 2 made for this report. The corresponding 171 adsorption energies can be found in Appendix B.

Table 2: List of Adsorbates and Bimetals

Adsorbates	**Bimetals**	
H	Mo_3Pd	Hf_3Au
N	Pd_3Sc	Pd_3Ag
N_2	Ag_3Mo	Hf_3Ag
NH	Ag_3Pd	Pd_3Ru
NH_2	Mo_3Ag	Cu_3Ru
NH_2NH_2	Ru_3Mo	Ta_3Ag
NH_3	Pd_3Mo	Ag_3Cu
NHNH	Ta_3Pd	Pd_3Ta
NNH	Mo_3Ru	Cu_3Pd
		Cu_3Ag

3.2 Paper 2

"Zinc dialkyl dithiophosphate adsorption and dissociation on ferrous substrates: An ab initio study"

In this ab initio study [4], the goal was to understand better the underlying mechanisms of the formation process of zinc dialkyl dithiophosphate (ZDDPs) tribofilms on iron. ZDDPs have been quite common as anti-wear additives in lubrication bearings. In the paper, extensive DFT calculations are made to obtain insights into the presence of oxygen on the adsorption energy between a ZDDP molecule and an iron (110) surface. The choice for this baseline was made to show how the limitation of the model. The ZDDP molecule as chosen as the adsorbate due to its relevance bearing lubrication.

3.2.1 DFT settings

The relevant calculations in the paper were performed using spin-polarised DFT, they implemented this with version 6.8 of the Quantum espresso suite [46], with the PBE GGA [17] exchange correlations functional. They chose the Hubbard U correction parameter to be 4.2 eV. The more specific DFT settings, Kinetic energy cutoff of 40 Ry, cutoff for charge densities 320 Ry, and A Gaussian smearing with a worst of 0.001 Ry were included by them to better represent occupations around the Fermi level. The electronic configuration of atoms was defined using ultrasoft pseudopotentials in the RRKJ [47] parametrisation. The threshold for the energy was set to 1×10^{-4} eV and that of forces to 1×10^{-3} eV Å^{-1}, which are the default convergence threshold criteria.

3.2.2 Structure definition

A large 6 x 4 orthorhombic supercell containing 48 atoms per layer for iron and oxygenated slabs was defined. A void of at least 10 Å was included to avoid interactions by vertical replicas. Relaxing the supercell resulted in the dimension 17.10 Å × 16.12 Å × 30.78 Å. A Γ point sampling of the Brillouin

zone was used. The adsorption energies were calculated according to the following:

$$E_{\text{ads}} = E_{\text{tot}} - (E_{\text{surf}} + E_{\text{adsorbate}}) \tag{9}$$

Where again E_{tot} is the energy of the total system, E_{surf} is the energy of only the bulk, $E_{adsorbate}$ is the gas state energy of the molecule, and E_{ads} is the adsorption energy. Locating the optimal adsorption site was done via Xsorb [48].

The two lateral alkyl chains were reduced to methyl groups to reduce the computational cost of the calculations; this was validated in their previous work [49]. The paper discussed various adsorption energies related to ZDDPs; however, for this report, the interest lies with the adsorption energy of a ZDDP molecule on a clean Fe (110) surface. This can be seen in Subfigure a and e of Figure 3. The adsorption energy calculated is $E_{ads} = -1.03\,\text{eV}$.

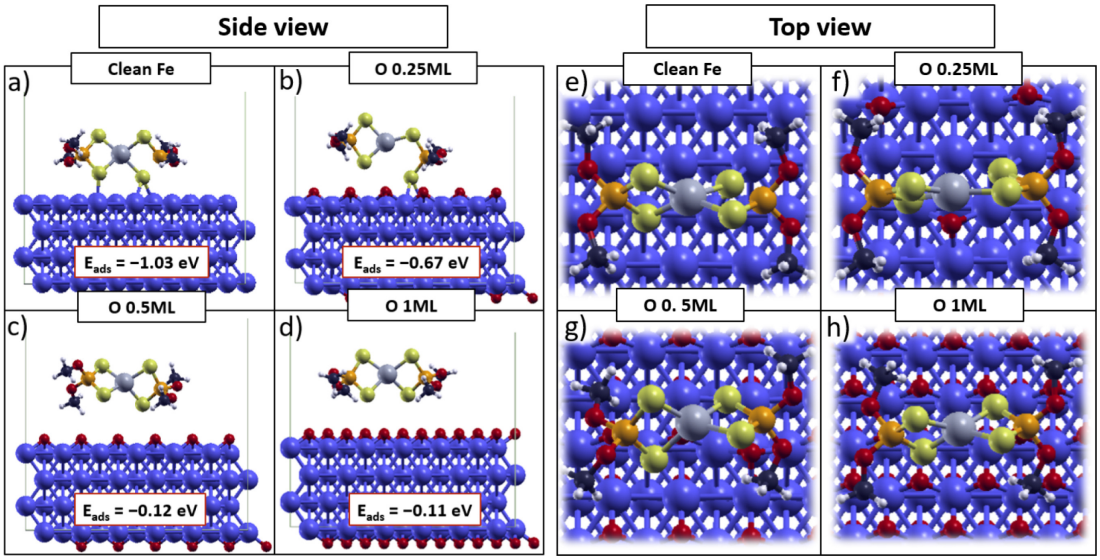

Figure 3: ide (left) and top (right) view of ZDDP adsorption on (a), (e) clean Fe and O passivated Fe with three different O coverages: (b), (f) 0.25 ML, (c), (g) 0.5 ML and (d), (h) 1 ML respectively. Adsorption energies are also reported. With P, Zn, C, H and S atoms are represented in orange, grey, black, white and yellow, respectively. Figure and caption is taken from Benini et al. [4].

4 Methodology

4.1 Computational specifications

All calculations are performed on a consumer-level GPU, a Nvidia GeForce RTX 2060. This choice aims to demonstrate the potential of models by performing these relaxations within a reasonable time frame on a consumer-level GPU. The primary measure of computational performance for GPUs is the Floating Point Operations Per Second (FLOPS). The RTX 2060 delivers approximately 6.45 TFLOPS with 1920 Cuda cores. This can be compared to the specs of the high-performance computing cluster of the University of Groningen, Hábrók. A single node of Hábrók is equipped with a Nvidia A100 GPU, which delivers approximately 19.49 TFLOPS with 6912 cores. This results in the statement that a general high-performance computer like Hábrók would be about a factor of three faster than the computations performed in this report.

4.2 Structure relaxations

Two sets of simulations will demonstrate the capabilities and limitations of the Open Catalyst Project pre-trained models. Both sets of calculations will be performed with the EquiformerV2 [12] and the GemNet-OC-Large [13] models. The first simulation is composed of 9 x 9 x 19 relaxations of nitrogen base molecules on bimetallics. These relaxations were chosen to show the known capabilities of the pre-trained models, as most of the metallic compounds used to train the models were binary metals. The second simulation will perform the relaxation of a ZDDP molecule on an iron bcc(110) surface. This was chosen to investigate the capability of the interatomic potentials to extrapolate to systems not considered during training.

4.3 OCPCalculator

The models can be accessed through the Fairchem python package operating with Atomic Simulation Environment (ASE) [50]. In this module, the OCPCalculater function is required to gain access to the models. The file path to the Fairchem database's pre-trained model must be specified. The Calculator then is attached to an ase object on which a Broyden–Fletcher–Goldfarb–Shanno (BFGS) [51] optimisation is performed. BFGS is a numerical optimisation algorithm for solving unconstrained non-linear optimisation problems that iteratively builds up an approximation to the Hessian matrix of the objective function in order to determine the minimum energy. A minimum force, after which the system is considered to be converged, has to be supplied together with a maximum number of steps for the optimisation to run.

4.4 Ammonia Nitrogen Reduction Reactions

The structures for the nitrogen reduction reactions simulations were obtained from the database provided by Fairchem. The 19 bimetallic compounds in question were optimised with single-point DFT calculations by Fairchem. For each compound, nine adsorption sites were located and placed with Pymatgen [52] on the (111) faces, and this resulted in ASE [50] structures, which is the required data type for the OCPCalculator function, resulting in a total of 9 x 9 x 19 relaxations. The adsorption sites are presented in Figure 4. The minimum energy required for the system to be considered converged is set to $0.03\,\mathrm{eV\,\AA^{-1}}$; this value was chosen because it is the same value as selected in the DFT calcula-

tions on which the dataset is trained [11]. The maximum number of steps for relaxation is set to 100. The relaxation trajectories are stored in an XYZ file format, allowing visualisation in OVITO [53].

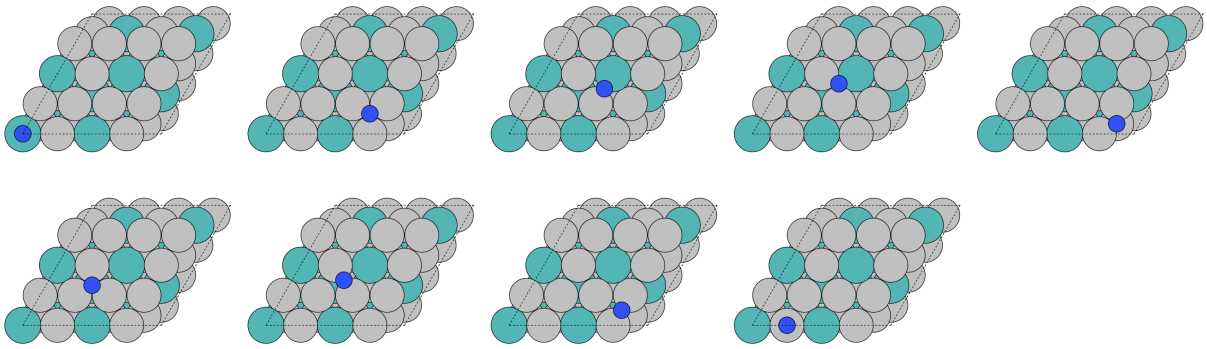

Figure 4: The nine adsorption sites used in the bimetallic relaxations. The example shown consists of a (111) surface of Ag_3Mo together with a nitrogen atom as adsorbate. Ag, Mo an d N are shown in grey, teal and blue, respectively

4.5 Fe(110) ZDDP

A similar method is used for the relaxation of the reduced ZDDP molecule. Initially, a Fe Body Centered Cubic (110) surface is defined with the ASE builder. The cell is defined with a size of (6 x 4 x 4), therefore containing 48 atoms for every 4 layers, similar to the ZDDP adsorption study [4]. All layers of atoms except the surface layer are constrained to their location; this decision was made because the same constraints were placed on the dataset on which the ML models were trained. The surface structure is relaxed initially to minimize the effects of surface restructuring during the actual relaxation. The ZDDP molecule is placed on the surface with the ASE package, and as with the previous simulations the relaxation is performed with the BGFS [51] optimisation algorithm. Again, the minimum energy is set to $0.03\,\mathrm{eV\,\AA^{-1}}$, with a maximum number of steps of 1000.

5 Results and Discussion

5.1 Nitrogen reduction reaction

A screening of various bi-metallic catalyst is set up in order to show the current capabilities of the pre-trained models. In total for all 9 adsorbates, 9 relaxations were performed on all possible adsorption sites. This was repeated for all 19 bi-metallic compounds. Anomalies resulting from improper relaxations were discarded. These anomalies consist of:

1. The adsorbate dissociating, meaning that the adsorbate breaks apart into smaller components.
2. The adsorbate being desorbed, meaning that the adsorbate are not adsorbed, but released back into the surrounding environment.
3. The surface has changed, which would result in a false adsorption energy.
4. The adsorbate is intercalated, meaning that the adsorbate is inserted into the layers of a nimetal.

The lowest energy for every combination of adsorbate and catalyst was selected and plotted, in order to compare the obtained adsorption energies to the literature values [42]. Three configurations were filtered out for both models. These filtered-out configurations consist of NH_2NH_2 on Ag_3Pd, N_2 on Ag_3Cu, and N_2 on Cu_3Ag, where all 9 relaxations for each configuration resulted in a desorption of the adsorbate.

5.1.1 EquiformerV2

In Figure 5, a total of 168 energies are presented. Three of the adsorbate-bimetal configurations were filtered out as mentioned in the previous section. All relaxations were performed in approximately 5.5 hours, resulting in an average of 115 seconds per unique adsorbate metal configuration.

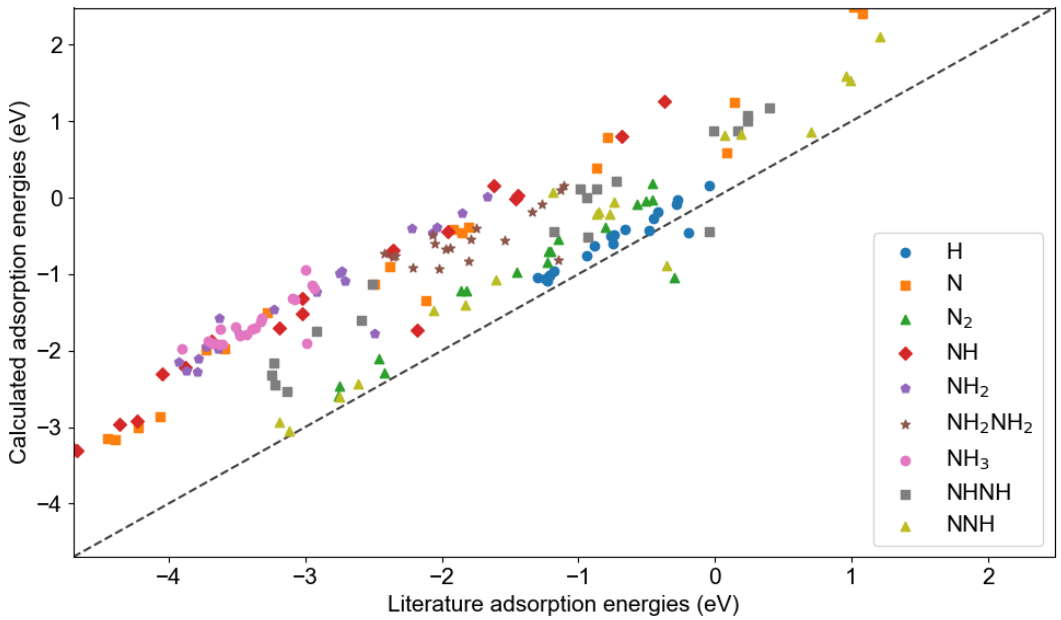

Figure 5: The calculated adsorption energies of nitrogen-based adsorbates on 19 different bimetallic compounds, compared to literature values taken from [42], calculated with EquiformerV2, with the line y = x to visualise the deviation.

Evident from the graph, the data does follow the same trend. However, a noticeable shift in the calculated values is apparent, ranging from 0 to 2 eV. The main reason expected to be the cause for this shift is the difference in DFT setting between the Open Catalyst Project [29], and the literature values [54]. The difference in exchange correlations between the dataset and the literature values is expected to influence this shift majorly. The Open Catalyst dataset is obtained with RPBE in contrary to the literature values, which are obtained with PBE.

The Mean Absolute Error of the adsorption energy for all relaxations is presented in Table 3 and is calculated to be 1.0669 eV; this is significantly higher than the presented MAE on the leaderboard of 0.3009 eV [39]. As mentioned, this shift is mainly expected to be a result of the difference in DFT settings, with a major influence of exchange-correlation functional, but also the effects of the general DFT settings, as they were selected in Open Catalyst with a focus on high throughput efforts.

Table 3: Total Mean Absolute Error (MAE) obtained with EquiformerV2

Description	**MAE**
Total MAE	1.0669

Table 4: MAE for Each Adsorbate obtained with EquiformerV2

Adsorbate	**MAE**
H	0.2059
N	1.3282
N2	0.4642
NH	1.4997
NH2	1.6612
NH2NH2	1.2546
NH3	1.7371
NHNH	0.8623
NNH	0.5356

Table 5: MAE for Each Composition obtained with EquiformerV2

Composition	**MAE**
Mo3Pd	1.1540
Pd3Sc	1.0886
Ag3Mo	0.5906
Ag3Pd	1.1128
Mo3Ag	1.2445
Ru3Mo	1.0677
Pd3Mo	1.1834
Ta3Pd	1.0488
Mo3Ru	1.2780
Hf3Au	0.9481
Pd3Ag	1.0598
Hf3Ag	0.8965
Pd3Ru	1.1726
Cu3Ru	1.1349
Ta3Ag	1.0073
Ag3Cu	1.1759
Pd3Ta	1.0750
Cu3Pd	0.9530
Cu3Ag	1.1010

5.1.2 GemNet-OC-Large

An equal amount of energies were discarded from the calculations of GemNet-OC-Large, the 168 eneriges are presented in Figure 6. The Figure is visually similar to the Figure 5, however when analysing the MAE, a slight difference is apparent. The MAE values are presented in Table 6. Here the total MAE is calculated to be 1.1066 eV, which is a larger value compared to the leaderboard of 0.3477 eV [39], showing a discrepancy between the obtained results, and the expected performance, indicating possible errors in the definition the calculations or the model. GemNet-OC-Large resulted in a larger total computation time of approximately 7 hours, averaging 150 seconds per unique combination.

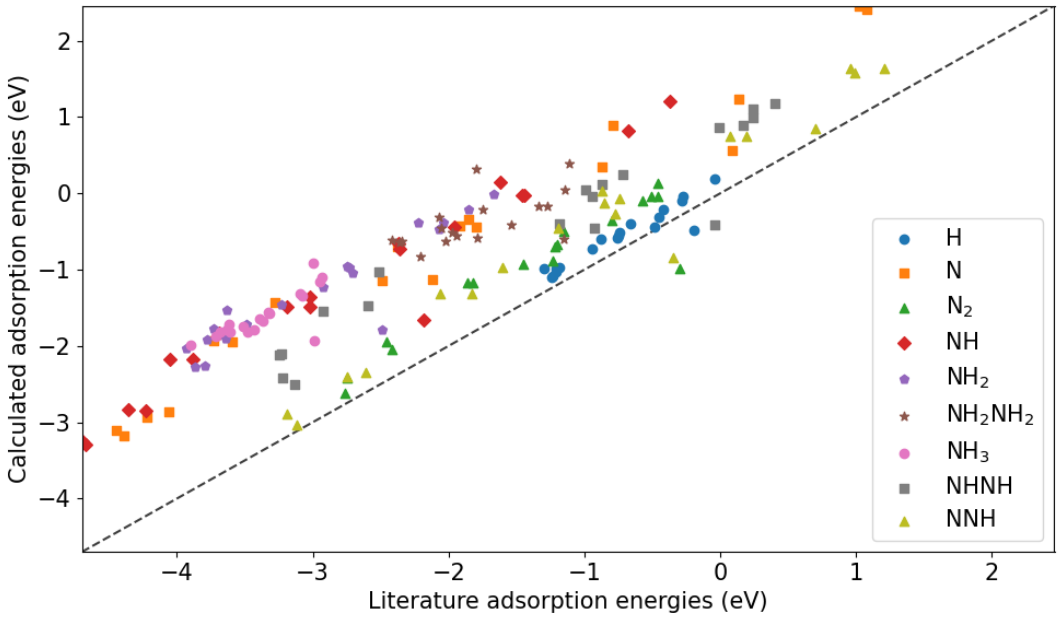

Figure 6: The calculated adsorption energies of nitrogen-based adsorbates on 19 different bimetallic compounds, compared to literature values taken from [42], calculated with GemNet-OC-Large, with the line y = x to visualise the deviation.

5.1.3 Nitrogen Reduction Reaction Discussion

All values derived with the pre-trained models present higher adsorption energies compared to the literature values [42]. There are multiple reasons that might explain this difference:

- The difference in exchange level theory between the dataset and the paper can account for about 0.5 eV, as mentioned in Section 2.2.
- The force setting after which the system is considered converged, as this threshold is much lower in the literature paper.
- The difference in general DFT (Density Functional Theory) settings.

Interestingly, despite considerable value deviations, the EquiformerV2 model displays a lower MAE than the GemNet-OC-Large. This is in accordance with the leaderboard, where the Equiformer is

Table 6: Total Mean Absolute Error (MAE) obtained with GemNet-OC-Large

Description	MAE
Total MAE	1.1066

Table 7: MAE for Each Adsorbate obtained with GemNet-OC-Large

Adsorbate	MAE
H	0.2045
N	1.3669
N2	0.4926
NH	1.5351
NH2	1.6974
NH2NH2	1.4267
NH3	1.7605
NHNH	0.9022
NNH	0.5261

Table 8: MAE for Each Composition obtained with GemNet-OC-Large

Composition	MAE
Mo3Pd	1.2215
Pd3Sc	1.1204
Ag3Mo	0.6301
Ag3Pd	1.1115
Mo3Ag	1.3522
Ru3Mo	1.1115
Pd3Mo	1.2621
Ta3Pd	1.1323
Mo3Ru	1.3544
Hf3Au	1.0037
Pd3Ag	1.0343
Hf3Ag	0.9064
Pd3Ru	1.1964
Cu3Ru	1.0881
Ta3Ag	1.1549
Ag3Cu	1.1498
Pd3Ta	1.1647
Cu3Pd	0.9343
Cu3Ag	1.1015

expected to perform slightly better than GemNet-OC-Large. Although the accuracy of these models falls short of what is required for reliable predictions, in the screening of catalyst, the required accuracy should be at least 0.1 eV [15]. However, apart from the lack of accuracy, the computational efficiency should not go unnoticed. The average computational times of 115 and 150 seconds recorded per unique combination are two orders of magnitude smaller than the approximately 24 [15] hours required for Density Functional Theory (DFT) calculations, and this was on a consumer grade-GPU, with computational speeds lower by a factor of 3. This considerable reduction in computational time depicts the potential of these models; however, much research is needed to use them in practice.

5.2 ZDDP adsorption on Iron (110) surface

An attempt to test the both the models their performance outside of their known capabilities is presented. Four relaxed structures of a ZDDP molecule on an iron (110) surface are presented. The simulations four relaxations were performed with identical settings, except for a small difference in the starting position of the ZDDP molecule.

5.2.1 EquiformerV2

Initially, the structure is relaxed without adding the ZDDP molecule to reduce the effects of surface reconstruction during the combined relaxation. It is not obvious; however, in Figure 7, the top layer is slightly attracted to the bulk structure. The relaxations with the ZDDP molecule added resulted in overly large and nonphysical adsorption energies of around $-25\,\text{eV}$. This is much larger than the expected value of $1.03\,\text{eV}$. The energy was expected to be off because ZDDP contains atoms that are not present in the adsorbate list of the dataset on which the model is trained. Figure of 8 showcases four final structures. Figure 8a presents the simulation box. Figure 8b depicts a dissociation and desorption of the remaining molecule. Both Figure 8c and 8d show a complete dissociation of the molecule. It's important to note that none of these relaxation processes can be considered correct due to the dissociations in the majority of relaxations.

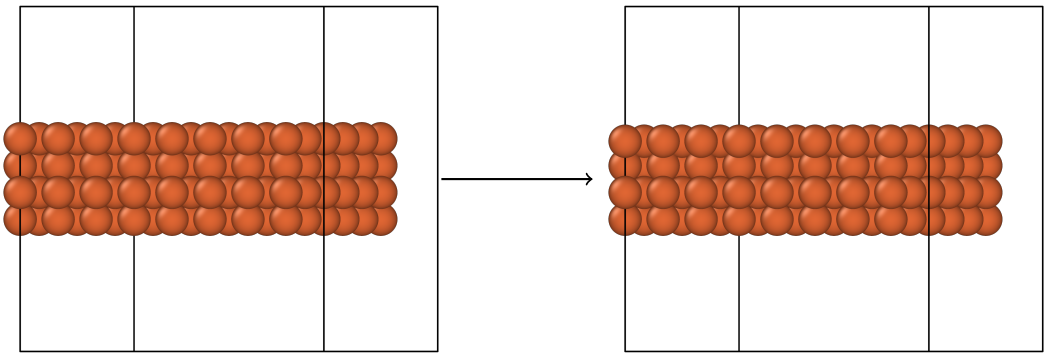

Figure 7: Front view of the initial structure (left) and the relaxed structure (right) performed with the EquiformerV2 model showcasing the slight height difference in the top layer.

5.2.2 GemNet-OC-Large

Similarly, the relaxation processes applied to the GemNet-OC-Large model yielded comparable results. However, the initial structure, as shown in Figure 9, was significantly deformed, indicating a possible limitation in the model's ability to form a BCC iron bulk structure. This is a crucial finding that underscores the model's constraints. A possible reason for this can come from the dataset generation of Open Catalyst, as mentioned in Section 2.4.1, no spin polarization was included in the generation of the Open Catalyst dataset. Spin polarisation, however, is critical in the formation of an iron bcc structure [55, 56].The final relaxations, as seen in Figure 10, were comparable to those of the Equiformer model. Where Figure 8a depicts the simulation box, and Figure 10b likewise depicts a dissociation and desorption of the remaining molecule. And again, both Figure 8c and 8d show a complete dissociation of the molecule.

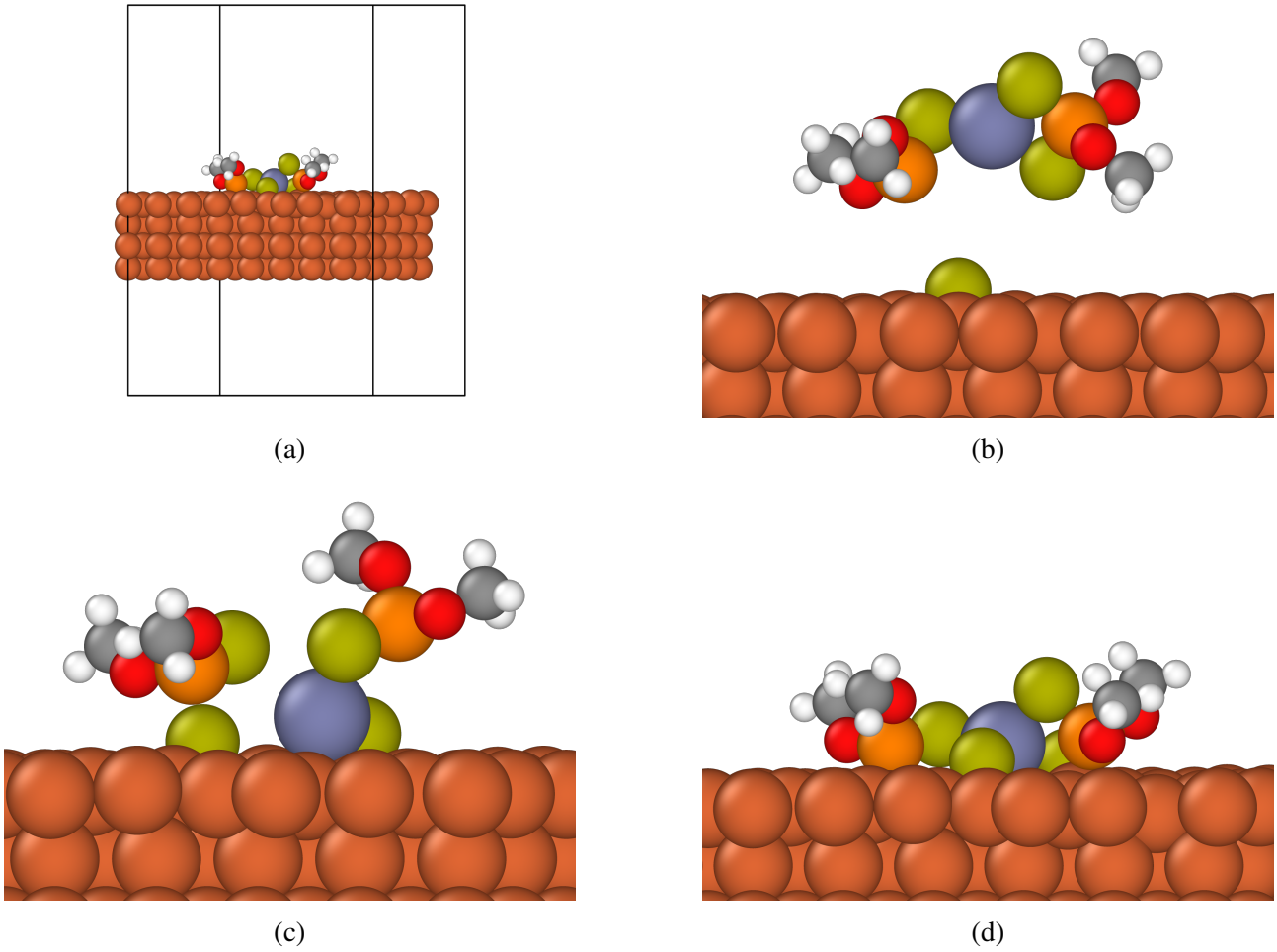

(a) (b) (c) (d)

Figure 8: Final structures after failed relaxation of a ZDDP molecule placed on a Fe bcc (110) surface performed with the EquiformerV2 model, showcasing dissociation and desorption. Where (a) presents the simulation box, and (b,c,d) depicts zoomed-in visualisations of the failed adsorptions.

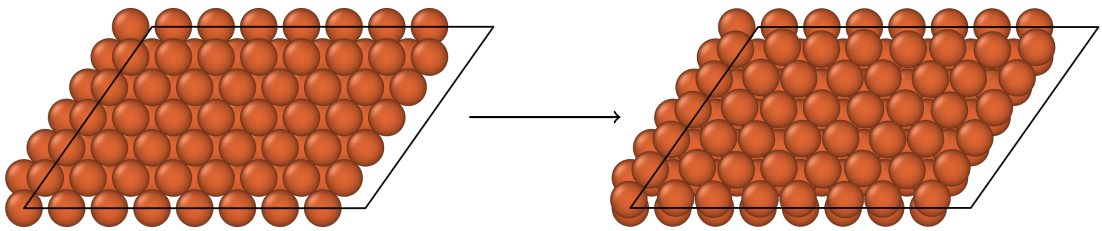

Figure 9: Top view of the initial structure (left) and the relaxed structure (right) performed with the GemNet-OC-Large model

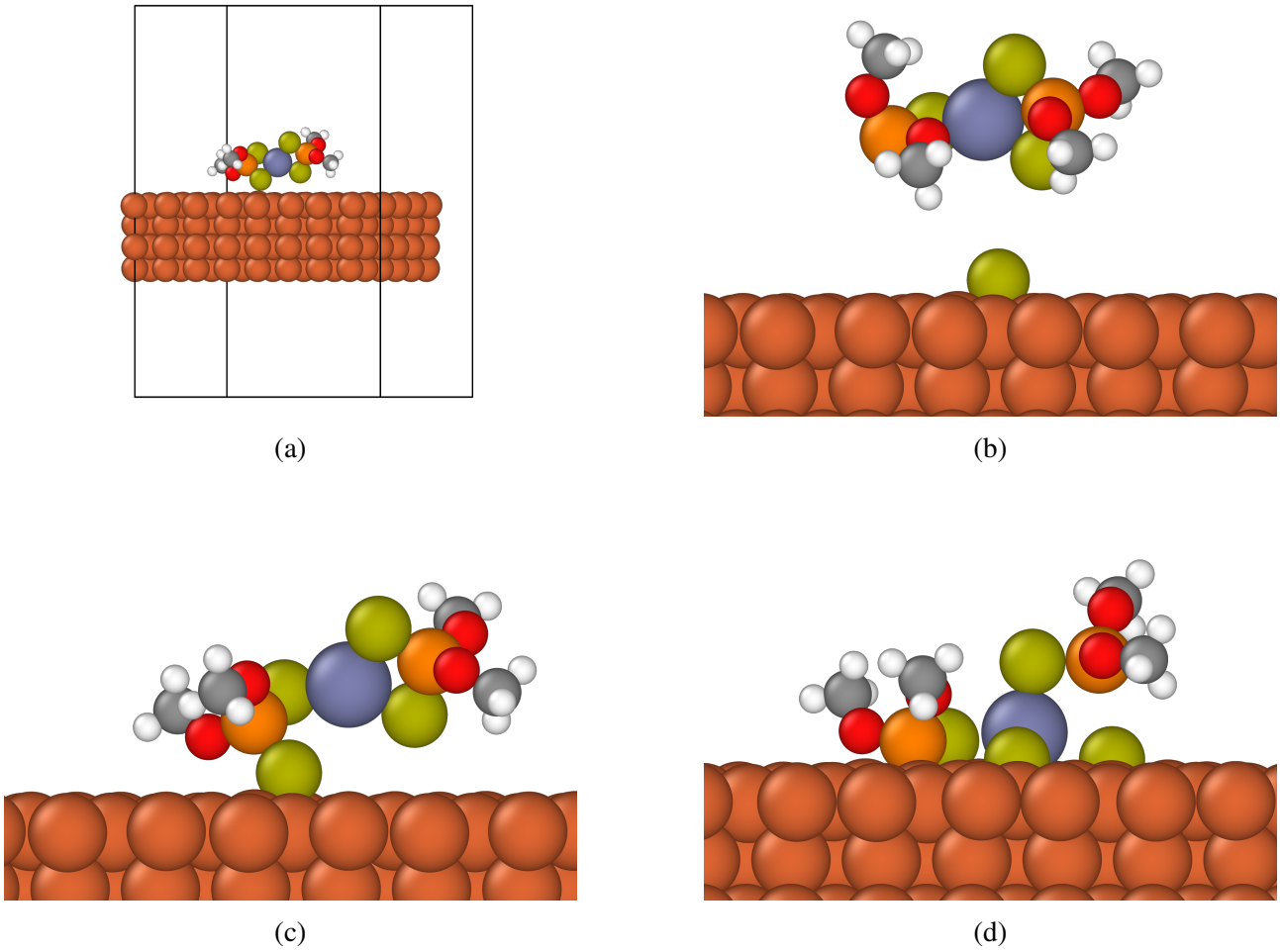

(a) (b) (c) (d)

Figure 10: Final structures after failed relaxation of a ZDDP molecule placed on a Fe bcc (110) surface performed with the EGemNet-OC-Large model, showcasing dissociation and desorption. Where (a) presents the simulation box, and (b,c,d) depicts zoomed-in visualisations of the failed adsorptions.

5.2.3 ZDDP adsorption on Iron (110) surface discussion

The attempt to calculate the adsorption energy of a more complicated molecule as ZDDP proves to be far beyond the capabilities of the currently available trained models. This aligns with the expectations based on Section 2.4.1 as the adsorbates in the dataset only contain oxygen, hydrogen, nitrogen and carbon. Currently, the models are not accurate enough to predict these calculations. A more specific dataset would be required to compute a complex molecule's adsorption energies as ZDDP.

6 Conclusion

In total, 1539 atomic relaxations were performed by both models to investigate the accuracy and time computational of two Open Catalyst pre-trained machine learning models. For EquiformerV2 and MAE, the energy was found to be 1.0669 eV with an average computational time of 115 seconds per unique configuration. GemNet-OC-Large performed slightly worse with an MAE of 1.1066 eV and an average time of 150 seconds per unique configuration. These errors are excessively large to make accurate surface property predictions; however, the reduced computational times demonstrate significant potential for greater-scale calculations that require less precision.

An attempt to derive the adsorption energy of a ZDDP on a molecule on an Iron bcc (110) surface revealed the models' current limitations. The relaxations led to either a dissociated or desorbed final structure, indicating that the models are not yet capable of accurately predicting this specific interaction.

The EquiformerV2 and GemNet-OC-Large are still in the early stages of their development; the accuracies still need to be higher when going outside the exact calculations in their dataset. As mentioned, these models have great potential, but the technology is still in the early phase. They could, however, be ideally utilized in combination with DFT, significantly speeding up the process but keeping some accuracy from DFT. It is also great to see the progress that Open Catalyst is making, as their goal is not to deliver great models but to accelerate the research in these models, and they are clearly showing great efforts to do this.

The EquiformerV2 and GemNet-OC-Large models are evidently in the early stages of their development, with accuracies remaining low when applied beyond the calculations for which they were initially trained. As previously noted, these models hold significant potential. However, the journey of their evolution is just beginning. Nevertheless, they could be employed in combination with DFT to improve computational efficiency while maintaining the accuracy of DFT. Additionally, it is respectable to see the progression being made by Open Catalyst. Their main objective is not to produce state-of-the-art models but to accelerate research within this domain, and their efforts are depicted clearly.

Bibliography

[1] "Processes at solid surfaces," in *Atkins' Physical chemistry*, pp. 824 – 844, Oxford, United Kingdom ; New York, NY: Oxford University Press, eleventh edition ed., 2018.

[2] J. K. Nørskov, J. Rossmeisl, A. Logadottir, L. Lindqvist, J. R. Kitchin, T. Bligaard, and H. Jónsson, "Origin of the Overpotential for Oxygen Reduction at a Fuel-Cell Cathode," *The Journal of Physical Chemistry B*, vol. 108, pp. 17886–17892, Nov. 2004.

[3] F. M. Sapountzi, J. M. Gracia, C. K.-J. Weststrate, H. O. Fredriksson, and J. H. Niemantsverdriet, "Electrocatalysts for the generation of hydrogen, oxygen and synthesis gas," *Progress in Energy and Combustion Science*, vol. 58, pp. 1–35, Jan. 2017.

[4] F. Benini, P. Restuccia, and M. C. Righi, "Zinc dialkyldithiophosphates adsorption and dissociation on ferrous substrates: An *ab initio* study," *Applied Surface Science*, vol. 642, p. 158419, Jan. 2024.

[5] D. S. Sholl and J. A. Steckel, *Density functional theory: a practical introduction*. Hoboken, N.J.: Wiley, 2009. OCLC: 441874984.

[6] C. L. Zitnick, L. Chanussot, A. Das, S. Goyal, J. Heras-Domingo, C. Ho, W. Hu, T. Lavril, A. Palizhati, M. Riviere, M. Shuaibi, A. Sriram, K. Tran, B. Wood, J. Yoon, D. Parikh, and Z. Ulissi, "An Introduction to Electrocatalyst Design using Machine Learning for Renewable Energy Storage," Oct. 2020. arXiv:2010.09435 [cond-mat].

[7] M. González, "Force fields and molecular dynamics simulations," *École thématique de la Société Française de la Neutronique*, vol. 12, pp. 169–200, 2011.

[8] A. C. T. Van Duin, S. Dasgupta, F. Lorant, and W. A. Goddard, "ReaxFF: A Reactive Force Field for Hydrocarbons," *The Journal of Physical Chemistry A*, vol. 105, pp. 9396–9409, Oct. 2001.

[9] W. D. Cornell, P. Cieplak, C. I. Bayly, I. R. Gould, K. M. Merz, D. M. Ferguson, D. C. Spellmeyer, T. Fox, J. W. Caldwell, and P. A. Kollman, "A Second Generation Force Field for the Simulation of Proteins, Nucleic Acids, and Organic Molecules," *Journal of the American Chemical Society*, vol. 117, pp. 5179–5197, May 1995.

[10] F. Scarselli, M. Gori, Ah Chung Tsoi, M. Hagenbuchner, and G. Monfardini, "The Graph Neural Network Model," *IEEE Transactions on Neural Networks*, vol. 20, pp. 61–80, Jan. 2009.

[11] L. Chanussot, A. Das, S. Goyal, T. Lavril, M. Shuaibi, M. Riviere, K. Tran, J. Heras-Domingo, C. Ho, W. Hu, A. Palizhati, A. Sriram, B. Wood, J. Yoon, D. Parikh, C. L. Zitnick, and Z. Ulissi, "The Open Catalyst 2020 (OC20) Dataset and Community Challenges," *ACS Catalysis*, vol. 11, pp. 6059–6072, May 2021. arXiv:2010.09990 [cond-mat].

[12] Y.-L. Liao, B. Wood, A. Das, and T. Smidt, "EquiformerV2: Improved Equivariant Transformer for Scaling to Higher-Degree Representations," Mar. 2024. arXiv:2306.12059 [physics].

[13] J. Gasteiger, M. Shuaibi, A. Sriram, S. Günnemann, Z. Ulissi, C. L. Zitnick, and A. Das, "GemNet-OC: Developing Graph Neural Networks for Large and Diverse Molecular Simulation Datasets," Sept. 2022. arXiv:2204.02782 [cond-mat, physics:physics].

[14] E. Cancès and G. Friesecke, eds., *Density functional theory: modeling, mathematical analysis, computational methods, and applications*. Mathematics and molecular modeling, Cham: Springer, 2023.

[15] J. Lan, A. Palizhati, M. Shuaibi, B. M. Wood, B. Wander, A. Das, M. Uyttendaele, C. L. Zitnick, and Z. W. Ulissi, "AdsorbML: A Leap in Efficiency for Adsorption Energy Calculations using Generalizable Machine Learning Potentials," *npj Computational Materials*, vol. 9, p. 172, Sept. 2023. arXiv:2211.16486 [cond-mat].

[16] J. P. Perdew and Y. Wang, "Accurate and simple analytic representation of the electron-gas correlation energy," *Physical Review B*, vol. 45, pp. 13244–13249, June 1992.

[17] J. P. Perdew, K. Burke, and M. Ernzerhof, "Generalized Gradient Approximation Made Simple," *Physical Review Letters*, vol. 77, pp. 3865–3868, Oct. 1996.

[18] B. Hammer, L. B. Hansen, and J. K. Nørskov, "Improved adsorption energetics within density-functional theory using revised Perdew-Burke-Ernzerhof functionals," *Physical Review B*, vol. 59, pp. 7413–7421, Mar. 1999.

[19] P. Janthon, S. M. Kozlov, F. Viñes, J. Limtrakul, and F. Illas, "Establishing the Accuracy of Broadly Used Density Functionals in Describing Bulk Properties of Transition Metals," *Journal of Chemical Theory and Computation*, vol. 9, pp. 1631–1640, Mar. 2013.

[20] W. P. Krekelberg, J. Greeley, and M. Mavrikakis, "Atomic and Molecular Adsorption on Ir(111)," *The Journal of Physical Chemistry B*, vol. 108, pp. 987–994, Jan. 2004.

[21] J. A. Herron, S. Tonelli, and M. Mavrikakis, "Atomic and molecular adsorption on Pd(111)," *Surface Science*, vol. 606, pp. 1670–1679, Nov. 2012.

[22] D. C. Ford, Y. Xu, and M. Mavrikakis, "Atomic and molecular adsorption on Pt(111)," *Surface Science*, vol. 587, pp. 159–174, Aug. 2005.

[23] M. Mavrikakis, J. Rempel, J. Greeley, L. B. Hansen, and J. K. Nørskov, "Atomic and molecular adsorption on Rh(111)," *The Journal of Chemical Physics*, vol. 117, pp. 6737–6744, Oct. 2002.

[24] S. Chmiela, A. Tkatchenko, H. E. Sauceda, I. Poltavsky, K. T. Schütt, and K.-R. Müller, "Machine learning of accurate energy-conserving molecular force fields," *Science Advances*, vol. 3, p. e1603015, May 2017.

[25] A. Duval, S. V. Mathis, C. K. Joshi, V. Schmidt, S. Miret, F. D. Malliaros, T. Cohen, P. Liò, Y. Bengio, and M. Bronstein, "A Hitchhiker's Guide to Geometric GNNs for 3D Atomic Systems," Mar. 2024. arXiv:2312.07511 [cs, q-bio, stat].

[26] T. M. Mitchell, "Does machine learning really work?," *AI Magazine*, vol. 18, p. 11, Sept. 1997.

[27] T. Xie and J. C. Grossman, "Crystal Graph Convolutional Neural Networks for an Accurate and Interpretable Prediction of Material Properties," *Physical Review Letters*, vol. 120, p. 145301, Apr. 2018.

[28] J. Hafner and G. Kresse, "The Vienna AB-Initio Simulation Program VASP: An Efficient and Versatile Tool for Studying the Structural, Dynamic, and Electronic Properties of Materials," in *Properties of Complex Inorganic Solids* (A. Gonis, A. Meike, and P. E. A. Turchi, eds.), pp. 69–82, Boston, MA: Springer US, 1997.

[29] L. Chanussot, A. Das, S. Goyal, T. Lavril, M. Shuaibi, M. Riviere, K. Tran, J. Heras-Domingo, C. Ho, W. Hu, A. Palizhati, A. Sriram, B. Wood, J. Yoon, D. Parikh, C. L. Zitnick, and Z. Ulissi, "The Open Catalyst 2020 (OC20) Dataset and Community Challenges," *ACS Catalysis*, vol. 11, pp. 6059–6072, May 2021. arXiv:2010.09990 [cond-mat].

[30] S. Ould Amrouche, D. Rekioua, T. Rekioua, and S. Bacha, "Overview of energy storage in renewable energy systems," *International Journal of Hydrogen Energy*, vol. 41, pp. 20914–20927, Dec. 2016.

[31] J. K. Nørskov, F. Studt, F. Abild-Pedersen, and T. Bligaard, *Fundamental concepts in heterogeneous catalysis*. Hoboken, New Jersey: Wiley, 2015.

[32] O. T. Holton and J. W. Stevenson, "The Role of Platinum in Proton Exchange Membrane Fuel Cells," *Platinum Metals Review*, vol. 57, pp. 259–271, Oct. 2013.

[33] A. D. Becke, "Perspective: Fifty years of density-functional theory in chemical physics," *The Journal of Chemical Physics*, vol. 140, p. 18A301, May 2014.

[34] M. S. Ziegler, J. M. Mueller, G. D. Pereira, J. Song, M. Ferrara, Y.-M. Chiang, and J. E. Trancik, "Storage Requirements and Costs of Shaping Renewable Energy Toward Grid Decarbonization," *Joule*, vol. 3, pp. 2134–2153, Sept. 2019.

[35] A. Jain, S. P. Ong, G. Hautier, W. Chen, W. D. Richards, S. Dacek, S. Cholia, D. Gunter, D. Skinner, G. Ceder, and others, "The materials project: A materials genome approach to accelerating materials innovation, APL Mater," 2013.

[36] J. R. Boes, O. Mamun, K. Winther, and T. Bligaard, "Graph Theory Approach to High-Throughput Surface Adsorption Structure Generation," *The Journal of Physical Chemistry A*, vol. 123, pp. 2281–2285, Mar. 2019. Publisher: American Chemical Society.

[37] M. Fey and J. E. Lenssen, "Fast Graph Representation Learning with PyTorch Geometric," Apr. 2019. arXiv:1903.02428 [cs, stat].

[38] A. Paszke, S. Gross, F. Massa, A. Lerer, J. Bradbury, G. Chanan, T. Killeen, Z. Lin, N. Gimelshein, L. Antiga, and others, "Pytorch: An imperative style, high-performance deep learning library," *Advances in neural information processing systems*, vol. 32, 2019.

[39] Open Catalyst Project, "Leaderboard," 2024.

[40] S. Passaro and C. L. Zitnick, "Reducing SO(3) Convolutions to SO(2) for Efficient Equivariant GNNs," June 2023. arXiv:2302.03655 [physics].

[41] J. Gasteiger, F. Becker, and S. Günnemann, "Gemnet: Universal directional graph neural networks for molecules," *Advances in Neural Information Processing Systems*, vol. 34, pp. 6790–6802, 2021.

[42] J. Zhou, X. Chen, M. Guo, W. Hu, B. Huang, and D. Yuan, "Enhanced Catalytic Activity of Bimetallic Ordered Catalysts for Nitrogen Reduction Reaction by Perturbation of Scaling Relations," *ACS Catalysis*, vol. 13, pp. 2190–2201, Feb. 2023.

[43] J. Hafner and G. Kresse, "The Vienna AB-Initio Simulation Program VASP: An Efficient and Versatile Tool for Studying the Structural, Dynamic, and Electronic Properties of Materials," in *Properties of Complex Inorganic Solids* (A. Gonis, A. Meike, and P. E. A. Turchi, eds.), pp. 69–82, Boston, MA: Springer US, 1997.

[44] S. Grimme, J. Antony, S. Ehrlich, and H. Krieg, "A consistent and accurate *ab initio* parametrization of density functional dispersion correction (DFT-D) for the 94 elements H-Pu," *The Journal of Chemical Physics*, vol. 132, p. 154104, Apr. 2010.

[45] H. J. Monkhorst and J. D. Pack, "Special points for Brillouin-zone integrations," *Physical Review B*, vol. 13, pp. 5188–5192, June 1976.

[46] P. Giannozzi, S. Baroni, N. Bonini, M. Calandra, R. Car, C. Cavazzoni, D. Ceresoli, G. L. Chiarotti, M. Cococcioni, I. Dabo, A. Dal Corso, S. De Gironcoli, S. Fabris, G. Fratesi, R. Gebauer, U. Gerstmann, C. Gougoussis, A. Kokalj, M. Lazzeri, L. Martin-Samos, N. Marzari, F. Mauri, R. Mazzarello, S. Paolini, A. Pasquarello, L. Paulatto, C. Sbraccia, S. Scandolo, G. Sclauzero, A. P. Seitsonen, A. Smogunov, P. Umari, and R. M. Wentzcovitch, "QUANTUM ESPRESSO: a modular and open-source software project for quantum simulations of materials," *Journal of Physics: Condensed Matter*, vol. 21, p. 395502, Sept. 2009.

[47] A. M. Rappe, K. M. Rabe, E. Kaxiras, and J. D. Joannopoulos, "Optimized pseudopotentials," *Physical Review B*, vol. 41, pp. 1227–1230, Jan. 1990.

[48] E. Pedretti, P. Restuccia, and M. C. Righi, "Xsorb: A software for identifying the most stable adsorption configuration and energy of a molecule on a crystal surface," *Computer Physics Communications*, vol. 291, p. 108827, Oct. 2023.

[49] S. Peeters, A. Barlini, J. Jain, N. N. Gosvami, and M. C. Righi, "Adsorption and decomposition of ZDDP on lightweight metallic substrates: Ab initio and experimental insights," *Applied Surface Science*, vol. 600, p. 153947, Oct. 2022.

[50] A. Hjorth Larsen, J. Jørgen Mortensen, J. Blomqvist, I. E. Castelli, R. Christensen, M. Dułak, J. Friis, M. N. Groves, B. Hammer, C. Hargus, E. D. Hermes, P. C. Jennings, P. Bjerre Jensen, J. Kermode, J. R. Kitchin, E. Leonhard Kolsbjerg, J. Kubal, K. Kaasbjerg, S. Lysgaard, J. Bergmann Maronsson, T. Maxson, T. Olsen, L. Pastewka, A. Peterson, C. Rostgaard, J. Schiøtz, O. Schütt, M. Strange, K. S. Thygesen, T. Vegge, L. Vilhelmsen, M. Walter, Z. Zeng, and K. W. Jacobsen, "The atomic simulation environment—a Python library for working with atoms," *Journal of Physics: Condensed Matter*, vol. 29, p. 273002, July 2017.

[51] J. D. Head and M. C. Zerner, "A Broyden—Fletcher—Goldfarb—Shanno optimization procedure for molecular geometries," *Chemical Physics Letters*, vol. 122, pp. 264–270, Dec. 1985.

[52] S. P. Ong, W. D. Richards, A. Jain, G. Hautier, M. Kocher, S. Cholia, D. Gunter, V. L. Chevrier, K. A. Persson, and G. Ceder, "Python Materials Genomics (pymatgen): A robust, open-source python library for materials analysis," *Computational Materials Science*, vol. 68, pp. 314–319, Feb. 2013.

[53] A. Stukowski, "Visualization and analysis of atomistic simulation data with OVITO–the Open Visualization Tool," *Modelling and Simulation in Materials Science and Engineering*, vol. 18, p. 015012, Jan. 2010.

[54] J. Zhang and H. Spikes, "On the Mechanism of ZDDP Antiwear Film Formation," *Tribology Letters*, vol. 63, p. 24, Aug. 2016.

[55] R. F. L. Evans, W. J. Fan, P. Chureemart, T. A. Ostler, M. O. A. Ellis, and R. W. Chantrell, "Atomistic spin model simulations of magnetic nanomaterials," *Journal of Physics: Condensed Matter*, vol. 26, p. 103202, Mar. 2014.

[56] K. Schwarz, P. Mohn, P. Blaha, and J. Kubler, "Electronic and magnetic structure of BCC Fe-Co alloys from band theory," *Journal of Physics F: Metal Physics*, vol. 14, pp. 2659–2671, Nov. 1984.

[57] I. Batatia, D. P. Kovács, G. N. C. Simm, C. Ortner, and G. Csányi, "MACE: Higher Order Equivariant Message Passing Neural Networks for Fast and Accurate Force Fields,"

Appendices

A MACE calculations

In addition, toward the end of the research, an attempt was made to perform an adsorption energy calculation with another equivariant machine learning software named MACE. This model was used to perform a calculation of of the adsorption energy of ZDDP on the hematite Fe_2O_3 (001) surface as presented in Benini et al. [4] and shown in Figure 11. Where MACE os an efficient equivariant message passing graph neural network with a high body order [57]. Citing Batatia et al. [57]:

> "As a result of the increased body order of the messages, only two message passing iterations are necessary to achieve high accuracy - unlike the typical five or six iterations of MPNNs, making it scalable and parallelizable. Finally, our implementation has remarkable computational efficiency, reaching state-of-the-art results on the 3BPA benchmark after 30 mins of training on NVIDIA A100 GPUs"

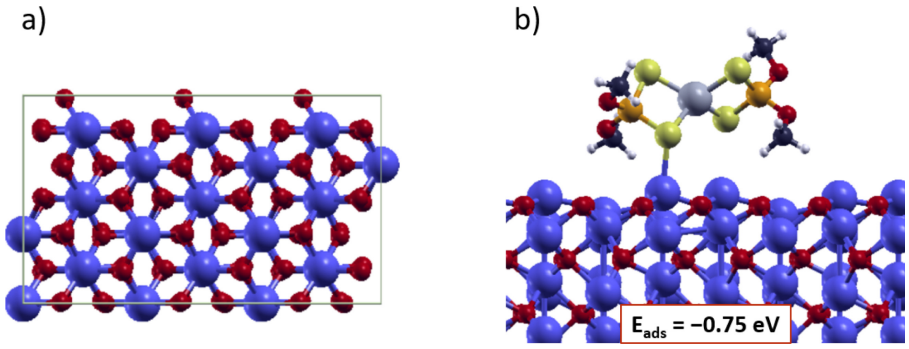

Figure 11: (a) Top view of the 3 × 2 supercell for the hematite (001) surface employed and side view of ZDDP adsorption on it (b). The adsorption energy value obtained is reported in panel (b). Figure and caption is taken from Benini et al. [4].

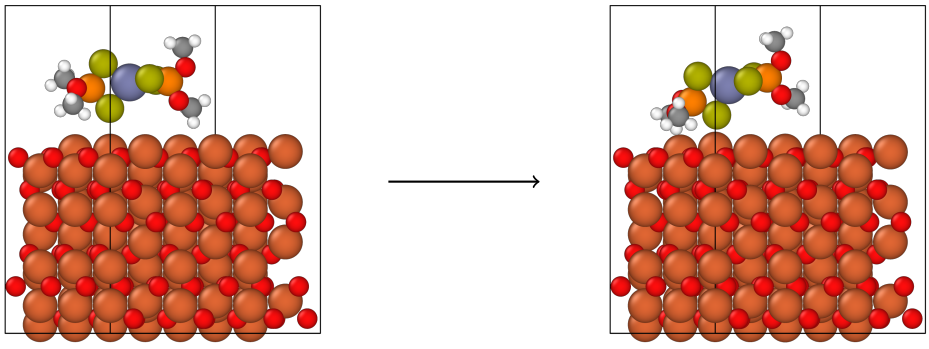

Figure 12: Front view of the initial structure (left) and the relaxed structure (right) of the Fe_2O_3 (001) ZDDP configuration performed with the MACE model indicating a correct structure relaxation.

The relaxations were set up identically to the paper. This model calculates the total energy of the system. Therefore, the adsorption energy was derived according to equation 1, where relaxations

were performed on the bulk, the molecule and the combination. By rotating the molecule for various initial positions, the minimum adsorption energy was obtained to be $-0.7940\,\text{eV}$, which is notably close to the presented $-0.75\,\text{eV}$. Figure 12 shows the initial state in Subfigure (a) and the relaxed state in Subgifure (b). These outcomes are presented to show that MACE delivered more promising results, and that MACE is a great model to perform further research on.

B Literature values

Table 9: Literature adsorption energies for Ag3Cu, Ag3Mo, Ag3Pd, Cu3Ag, and Cu3Pd compounds. [42]

Intermediate	Ag3Cu ΔE	Ag3Mo ΔE	Ag3Pd ΔE	Cu3Ag ΔE	Cu3Pd ΔE
N2	-0.21	-0.30	-0.57	-0.14	-0.46
NNH	1.21	-0.35	0.99	0.96	0.70
NNH2	0.71	-1.09	0.77	0.23	-0.09
NHNH	0.40	-0.04	0.24	0.24	0.17
NHNH2	-0.22	-0.77	-0.02	-0.76	-0.94
NH2NH2	-1.11	-1.15	-1.14	-1.13	-1.27
N	1.08	-2.12	1.02	0.14	0.09
NH	-0.68	-2.18	-0.37	-1.46	-1.62
NH2	-1.85	-2.49	-1.67	-2.07	-2.22
NH3	-2.95	-2.99	-3.00	-2.93	-3.08
H	-0.04	-0.19	-0.27	-0.28	-0.48

Table 10: Literature adsorption energies for Cu3Ru, Hf3Ag, Hf3Au, Mo3Ag, and Mo3Pd compounds. [42]

Intermediate	Cu3Ru ΔE	Hf3Ag ΔE	Hf3Au ΔE	Mo3Ag ΔE	Mo3Pd ΔE
N2	-1.23	-2.76	-2.75	-1.82	-1.86
NNH	-0.77	-3.12	-3.19	-2.06	-1.83
NNH2	-0.97	-3.46	-3.65	-3.02	-2.78
NHNH	-0.99	-3.13	-3.22	-2.92	-2.59
NHNH2	-1.39	-2.82	-2.89	-3.10	-2.65
NH2NH2	-1.79	-1.94	-2.02	-2.42	-2.05
N	-1.80	-4.39	-4.45	-3.73	-3.59
NH	-2.36	-4.67	-4.70	-4.05	-3.88
NH2	-2.73	-3.79	-3.87	-3.73	-3.49
NH3	-3.51	-3.43	-3.48	-3.61	-3.39
H	-0.76	-1.24	-1.23	-1.21	-1.18

Table 11: Literature adsorption energies for Mo3Ru, Pd3Ag, Pd3Mo, Pd3Ru, and Pd3Sc compounds. [42]

Intermediate	Mo3Ru ΔE	Pd3Ag ΔE	Pd3Mo ΔE	Pd3Ru ΔE	Pd3Sc ΔE
N2	-1.45	-0.46	-1.20	-1.22	-0.51
NNH	-1.60	0.19	-1.19	-0.74	0.07
NNH2	-2.77	-0.29	-1.90	-1.18	-0.59
NHNH	-2.51	-0.01	-0.94	-0.87	-0.72
NHNH2	-2.64	-0.70	-1.75	-1.28	-1.31
NH2NH2	-2.07	-1.34	-1.80	-1.97	-1.54
N	-3.28	-0.87	-2.38	-1.92	-0.79
NH	-3.69	-1.44	-3.02	-2.37	-1.96
NH2	-3.63	-2.04	-3.23	-2.75	-2.71
NH3	-3.33	-3.09	-3.71	-3.62	-3.37
H	-0.94	-0.74	-0.45	-0.66	-0.88

Table 12: Literature adsorption energies for Pd3Ta, Ru3Mo, Ta3Ag, and Ta3Pd compounds. [42]

Intermediate	Pd3Ta ΔE	Ru3Mo ΔE	Ta3Ag ΔE	Ta3Pd ΔE
N2	-1.15	-0.80	-2.42	-2.46
NNH	-0.87	-0.85	-2.75	-2.61
NNH2	-1.81	-1.61	-3.38	-3.54
NHNH	-0.93	-1.18	-3.25	-3.23
NHNH2	-2.22	-1.91	-3.00	-2.90
NH2NH2	-2.21	-1.75	-2.34	-2.36
N	-1.85	-2.49	-4.22	-4.06
NH	-3.19	-3.02	-4.36	-4.23
NH2	-3.64	-2.92	-3.78	-3.93
NH3	-3.90	-3.32	-3.63	-3.68
H	-0.42	-0.75	-1.30	-1.21